THE ASTROPHYSICAL JOURNAL, 556:70–76, 2001 July 20


# *HUBBLE SPACE TELESCOPE* STIS OBSERVATIONS OF GRB 000301C: CCD IMAGING AND NEAR-ULTRAVIOLET MAMA SPECTROSCOPY[1]

ALAIN SMETTE,[2,3] ANDREW S. FRUCHTER,[4] THEODORE R. GULL,[2] KAILASH C. SAHU,[4] LARRY PETRO,[4] HENRY FERGUSON,[4] JAMES RHOADS,[4] DON J. LINDLER,[5] RACHEL GIBBONS,[4] DAVID W. HOGG,[6] CHRYSSA KOUVELIOTOU,[7] MARIO LIVIO,[4] DUCCIO MACCHETTO,[4,8] MARK R. METZGER,[9] HOLGER PEDERSEN,[10] ELENA PIAN,[11] STEPHEN E. THORSETT,[12] RALPH A. M. J. WIJERS,[13] JOHAN P. U. FYNBO,[14] JAVIER GOROSABEL,[15] JENS HJORTH,[10] BRIAN L. JENSEN,[10] ALAN LEVINE,[16] DONALD A. SMITH,[16] TOM CLINE,[2] KEVIN HURLEY,[17] AND JACK TROMBKA[2]

*Received 2000 July 14; accepted 2001 March 9*

## ABSTRACT

We present Space Telescope Imaging Spectrograph observations of the optical transient (OT) counterpart of the $\gamma$-ray burster GRB 000301C obtained 5 days after the burst, on 2000 March 6. CCD clear-aperture imaging reveals a $R \simeq 21.50 \pm 0.15$ source with no apparent host galaxy. An 8000 s, 1150 Å $< \lambda <$ 3300 Å near-ultraviolet MAMA prism spectrum shows a flat or slightly rising continuum (in $f_\lambda$) between 2800 and 3300 Å, with a mean flux of $(8.7^{+0.8}_{-1.6} \pm 2.6) \times 10^{-18}$ ergs s$^{-1}$ cm$^{-2}$ Å$^{-1}$, and a sharp break centered at $2797 \pm 25$ Å. We interpret this as the H I Lyman break at $z = 2.067 \pm 0.025$, indicating the presence of a cloud with an H I column density $\log N_{\rm H\,I}({\rm cm}^2) > 18$ on the line of sight to the OT. This measured redshift is conservatively a lower limit to the GRB redshift. However, as all other GRBs that have deep *Hubble Space Telescope* images appear to lie on the stellar field of a host galaxy, and as the large H I column density measured here and in later ground-based observations is unlikely on a random line of sight, we believe we are probably seeing absorption from H I in the host galaxy. In any case, this represents the largest direct redshift determination of a $\gamma$-ray burster to date. Our data are compatible with an OT spectrum represented by a power law with an intrinsic index $\alpha = 1.2$ ($f_\nu \propto \nu^{-\alpha}$) and no extinction in the host galaxy, or with $\alpha = 0.5$ and extinction by SMC-like dust in the OT rest frame with $A_V = 0.15$. The large $N_{\rm H\,I}$ and the lack of a detected host are similar to the situation for damped Ly$\alpha$ absorbers at $z > 2$.

*Subject heading:* gamma rays: bursts

## 1. INTRODUCTION

Gamma-ray bursts (GRBs) remain mysterious nearly 30 years after their first detection (Klebesadel, Strong, & Olson 1973), although some progress has been made in understanding them. The large sample of events collected by the Burst and Transient Source Experiment (BATSE) on board the *Compton Gamma Ray Observatory* shows an isotropic angular distribution (Meegan et al. 1992). However, their intensity distribution shows fewer weak bursts than expected from a homogeneous distribution of sources in a Euclidean space. It was therefore thought that GRBs were of extragalactic origin (Meegan et al. 1992).

Rapidly distributed arcminute localizations derived from X-ray instruments such as those on the *BeppoSAX* (Costa et al. 1997) and, more recently, *Rossi X-Ray Timing Explorer* (*RXTE*; Smith et al. 1999) satellites have revealed the exis-

[1] Based on observations with the NASA/ESA *Hubble Space Telescope*, obtained at the Space Telescope Science Institute, which is operated by the Association of Universities for Research in Astronomy, Inc., under NASA contract NAS 5-26555.
[2] NASA Goddard Space Flight Center, Greenbelt, MD 20771; asmette@band3.gsfc.nasa.gov, gull@sea.gsfc.nasa.gov, cline@lheavx.gsfc.nasa.gov, u1jit@lepvax.gsfc.nasa.gov.
[3] National Optical Astronomy Observatories, 950 North Cherry Avenue, Tucson, AZ 85726-6732; and Collaborateur Scientifique, Fonds National de la Recherche Scientifique, Belgium.
[4] Space Telescope Science Institute, 3700 San Martin Drive, Baltimore, MD 21218; fruchter@stsci.edu, sahu@stsci.edu, petro@stsci.edu, ferguson@stsci.edu, rhoads@stsci.edu, gibbons@stsci.edu, livio@stsci.edu, macchetto@stsci.edu.
[5] Advanced Computer Concepts, Inc., Code 681, Goddard Space Flight Center, Greenbelt, MD 20771; lindler@rockit.gsfc.nasa.gov.
[6] Institute for Advanced Study, Einstein Drive, Princeton, NJ 08540; and Hubble Fellow; hogg@ias.edu.
[7] NASA Marshall Space Flight Center, ES-84, Huntsville, AL 35812; and Universities Space Research Association; chryssa.kouveliotou@msfc.nasa.gov.
[8] Astrophysics Department, Space Science Division, European Space Agency, Keplerlaan 1, Postbus 299, NL-2200 AG Noordwijk, Netherlands.
[9] Department of Astronomy, MS 105-24, California Institute of Technology, Pasadena, CA 91125; mrm@grus.caltech.edu.
[10] Astronomical Observatory, University of Copenhagen, Juliane Maries Vej 30, D-2100 Copenhagen Ø, Denmark; holger@ursa.astro.ku.dk, jens@astro.ku.dk, brian_j@astro.ku.dk.
[11] Istituto di Tecnologie e Studio delle Radiazioni Extraterrestri, Consiglio Nazionale delle Ricerche, Via Gobetti 101, I-40129 Bologna, Italy; pian@tesre.bo.cnr.it.
[12] Department of Astronomy and Astrophysics, University of California, Santa Cruz, CA 95064; and Alfred P. Sloan Research Fellow; thorsett@ucolick.org.
[13] Department of Physics and Astronomy, State University of New York at Stony Brook, 452 Earth and Space Sciences Building, Stony Brook, NY 11794-3800; rwijers@ourania.ess.sunysb.edu.
[14] Institute of Physics and Astronomy, Åarhus University, DK-8000 Åarhus C., Denmark; and European Southern Observatory, D-85748 Garching bei München, Germany; jfynbo@ifa.au.dk.
[15] Danish Space Research Institute, Juliane Maries Vej 30, DK-2100 Copenhagen Ø, Denmark; jgu@dsri.dk.
[16] Center for Space Research, Massachusetts Institute of Technology, 77 Massachusetts Avenue, Cambridge, MA 02139; aml@space.mit.edu, dasmith@space.mit.edu.
[17] Space Sciences Laboratory, University of California, Berkeley, CA 94720-7450; khurley@ssl.berkeley.edu.

tence of fading afterglows and enabled efficient searches for GRB counterparts to be carried out at other wavelengths. The optical transient (OT) to GRB 970228 was the first to be discovered (van Paradijs et al. 1997). Its location, angularly close to a faint diffuse object, possibly a galaxy, suggested that the two objects are associated, providing further evidence that GRBs lie at cosmological distances (van Paradijs et al. 1997; Sahu et al. 1997; later, Fruchter et al. 1999a showed that the diffuse object is indeed a $V = 25.8$ galaxy). This hypothesis was soon confirmed when a direct spectrum of the OT to GRB 970508 revealed absorption lines at the same redshift as the underlying $z = 0.835$ galaxy (Metzger et al. 1997; Bloom et al. 1998). Since then, OTs have been found for roughly half of the GRBs for which an X-ray afterglow has been detected, and most of them appear to be associated with faint, $z > 0.4$ galaxies (Hogg & Fruchter 1999; Kulkarni et al. 2000). In particular, the probable host galaxy of GRB 971214 has a redshift of $z = 3.42$ (Kulkarni et al. 1998). Most popular theories describing the GRB phenomenon suggest that GRB activity will be closely tied in time to episodes of massive star formation.

The collapse of massive stars (Paczyński 1998) requires an active or recently active star-forming host, while most neutron star–neutron star or neutron star–black hole binary mergers (Paczyński 1991; Narayan, Paczyński, & Piran 1992) occur not long after star formation.

The evidence for such an environment is already suggestive, as a number of host galaxies show strong emission lines associated with star formation (Metzger et al. 1997; Djorgovski et al. 1998; Kulkarni et al. 1998; Bloom et al. 1999; Vreeswijk et al. 2001), while direct imaging with the *Hubble Space Telescope* (*HST*) Space Telescope Imaging Spectrograph (STIS) and Near Infrared Camera and Multi-Object Spectrometer indicates that they are unusually blue, with $V-H < 1$, whereas most galaxies in the Hubble Deep Field have $V-H > 1$ (Fruchter et al. 1999b). We thus expect that the spectra of OTs will show evidence that the events take place in environments of massive star formation: large hydrogen column density, large extinction by dust, or even absorption by molecular hydrogen (Draine 2000). All lead to features in the rest-frame UV region.

We have thus embarked on a program to obtain, as targets of opportunity, *HST* STIS near-ultraviolet spectra of GRB OTs. Although Bloom et al. (1997) have suggested using grating modes of STIS for studying GRBs, we chose to use the prism as it is the most efficient available spectral element due to its low dispersion and broad spectral coverage. Combined with the near-ultraviolet, photon-counting multianode microchannel array (NUV-MAMA) detector, the prism mode provides spectral coverage over the wavelength range 1150 Å $\lesssim \lambda \lesssim$ 3300 Å. However, its highly nonlinear dispersion makes the wavelength calibration at the red end (2800 Å $\lesssim \lambda \lesssim$ 3300 Å) especially critical.

Here we present *HST* STIS clear-aperture CCD imaging and the first ultraviolet spectrum of a GRB optical counterpart, GRB 000301C. This burst was detected at 9:51:37 (UTC) on 2000 March 1 by the all-sky monitor instrument aboard the *RXTE* satellite, as well as by the *Ulysses* GRB experiment and the *Near Earth Asteroid Rendezvous* (*NEAR*; Smith et al. 2000) X-ray/gamma-ray spectrometer in the Third Interplanetary Network. Its $\gamma$-ray light curve showed a common, simple shape: a singly peaked, fast rise followed by a slow decay lasting a total of 10 s, which qualifies it as a short-to-intermediate duration burst (Jensen et al. 2001). The resulting composite localization of area $\sim 50$ arcmin$^2$ was imaged on 2000 March 3.14–3.28 (UTC) by Fynbo et al. (2000a) with the Nordic Optical Telescope (NOT), which revealed a then $R = 20.09 \pm 0.04$, blue optical counterpart (Jensen et al. 2001).

All exposures were taken on 2000 March 6 (UTC) during a single, five-orbit visit. The first orbit was dedicated to imaging, acquisition, and calibration. Four 2000 s NUV-MAMA prism spectra were obtained during the subsequent four orbits.

## 2. IMAGING

The field of GRB 000301C was observed using the STIS 50CCD clear-aperture mode. In this setting no filter is interposed between the CCD and the sky, and the bandpass is determined entirely by the reflectivity of the optics and the response of the CCD. Three exposures of 480 s each were taken in a diagonal dither pattern and combined using the Drizzle algorithm and associated techniques (Fruchter & Hook 1999; Fruchter et al. 1997). The drizzled output image, presented in Figure 1, has pixels of one-half the linear dimensions of the original images, or 0.″025355 $\pm$ 0.″000035, since the pixel scale of the CCD is 0.″05071 $\pm$ 0.″00007 (Malumuth & Bowers 1997).

At the position of the optical transient of GRB 000301C, we find an unresolved object (FWHM 0.″087) whose appearance is consistent with the STIS CCD point-spread function (PSF). The mean count rate of detected photons within 20 CCD pixels (containing more than 99.6% of the flux; Leitherer et al. 2000) from the OT image centroid is 56.0 counts s$^{-1}$ on mean 2000 March 6.22 (UTC). Assuming a power-law spectrum with $\alpha = -0.8$ and a foreground Galactic extinction with $A_V = 0.16$, as determined from the dust

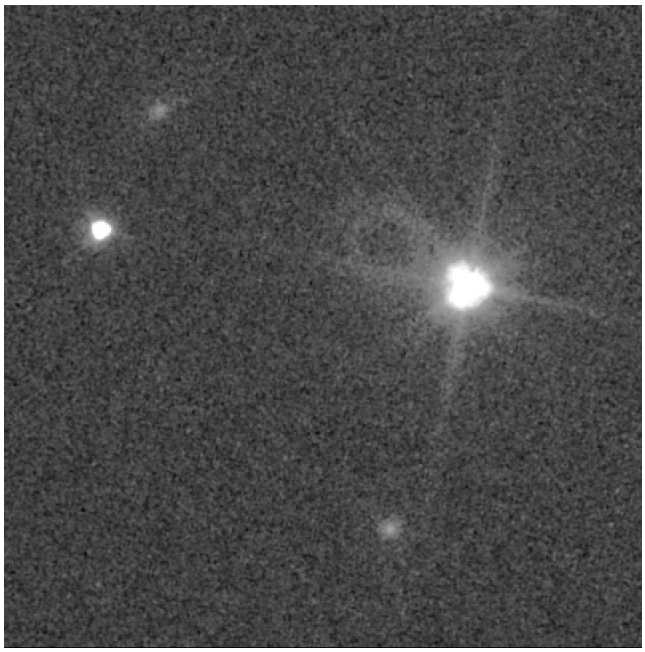

FIG. 1.—A 10″ × 10″ portion of the *HST* STIS clear-aperture CCD image of the field of GRB 000301C showing the OT on the left and the offset star used for acquisition on the right. North is up and east is to the left. The ring visible on the left of the offset star is a ghost due to internal reflections in the STIS CCD window.

extinction map given by Schlegel, Finkbeiner, & Davis (1998), we obtain a magnitude of $R = 21.5 \pm 0.15$, where the uncertainty is dominated by the fact that the STIS CCD clear-aperture mode is not completely calibrated.

Any underlying galaxy would have to have $R \gtrsim 24$, or be unusually compact, for it to avoid detection in our data. We therefore believe that the apparent flattening—the decrease of the OT luminosity fading rate—of the light curve in the $R$-band reported by many observers before this image was taken (e.g., Garnavich et al. 2000; Halpern et al. 2000a; Bernabei et al. 2000; Rhoads & Fruchter 2001 and references therein) is not due to an underlying host galaxy. Instead, it may be due either to the jet itself (Berger et al. 2000) or to microlensing (Garnavich, Loeb, & Stanek 2000).

The diffuse emission to the northwest of the OT is the galaxy previously identified as a possible host (Rhoads & Fruchter 2000). From our STIS image, we derived an AB magnitude of $25.1 \pm 0.2$ in the STIS clear-aperture passband. The lack of emission between the two, and the good fit between the OT and the STIS PSF, suggests that the OT host galaxy has not yet been detected.

## 3. SPECTROSCOPY

### 3.1. *Acquisition and Reduction*

In this section we describe the acquisition and the reduction procedures that required special attention. The reduction was performed using the interactive data language (IDL) and the Goddard Space Flight Center version of CALSTIS (Lindler 1999).[18]

Each TIME-TAG 2000 s spectrum was obtained with the prism using the 2125 Å setting, so that the spectral region corresponding to wavelengths of $\sim$2125 Å falls onto the central region of the NUV-MAMA detector, and the $52'' \times 0''.5$ slit. After each scientific spectrum an automatic wavelength calibration exposure was taken through the narrower $52'' \times 0''.05$ slit.

We used the $R = 18.05$ star located $\sim 5''.7$ west to the OT (see Fig. 1) as an offset star. The offset values were determined from the $3 \times 900$ s $R$-band NOT image. Acquisition took place after the STIS CCD imagery and just before the NUV-MAMA prism spectroscopy. This order allowed us to obtain the CCD images independently of the success of the spectral acquisition. However, as the acquisition produces a small change in the location of the object on the detector, an additional offset has to be taken into account for the zero-point determination of the wavelength calibration (see below).

Each scientific raw data set displays a spectrum whose spatial profile can be modeled by a Gaussian with a mean FWHM of 2.5 pixels, or $0''.072$, as expected from a point source. There is no significant variation in the count rate between the different data sets, as well as no significant variation in the count rate during the course of an orbit.

The sum of the sky and dark backgrounds at the location of the OT spectrum was determined for each individual exposure. It was obtained by interpolation based on a fifth-degree polynomial fitted independently to each column of the image, avoiding a 20 pixel wide region centered on the object spectrum. Extraction was performed by summing up seven rows centered on the peak of the two-dimensional spectrum.

[18] See http://hires.gsfc.nasa.gov/stis/software/calstis.html.

Each extracted spectrum was then wavelength calibrated. This step is especially critical, so we describe it here in more detail. The prism dispersion relation $\lambda = \lambda(X)$ gives the wavelength $\lambda$ corresponding to the pixel[19] number $X$ in the extracted spectrum. It is well modeled by a relation

$$\lambda = \sum_{i=0}^{4} \frac{a_i}{(X - X_0)^i} . \quad (1)$$

Because of the strong blending of the lines, especially at the red end of the spectrum, no determination of the dispersion solution (i.e., the values of each coefficient $a_i$) is feasible on-orbit. Instead, the values of $a_i$ were obtained during the prelaunch thermal vacuum testing of STIS using an external platinum discharge lamp fed through a vacuum monochromator, the $52'' \times 0''.05$ slit, and the same 2125 Å setting as for the observations. The residuals to the fit were then measured to have an rms equal to 0.16 pixels.

The quantity $X_0$ is, in pixels, the separation along the dispersion direction of the projected location of the object on the detector from the projected location of the center of the $52'' \times 0''.05$ slit used for the determination of the dispersion solution. $X_0$ determines the zero point of the wavelength calibration for each exposure and can be represented as the sum of three quantities: (1) $\Delta\phi_{\rm row}$, the difference in pixels between the angular separations along the dispersion direction between the OT and the offset star, as determined on the STIS CCD and NOT images; (2) $\Delta\chi$, the difference in pixels between the projection on the detector of the center of the slit used for the wavelength calibration relative to its location during the prelaunch calibration; (3) $\Delta\beta$, the difference in pixels between the location of the center of the slit used during the scientific exposures ($52'' \times 0''.5$) and that used for the automatic wavelength calibration after each scientific exposure ($52'' \times 0''.05$). In the following, we describe how each of these three quantities can be determined.

The acquisition process usually centers the object in the slit used for the scientific exposure. However, the nearby $R = 18.05$ bright star was considered too close to the OT and could have interfered with the normal procedure. Instead, it was used as an offset star. Consequently, the acquisition process (*a*) changed the spacecraft orientation so that the offset star is centered on the slit by an onboard centroid algorithm and then (*b*) modified the spacecraft pointing to take into account the offsets in right ascension and declination between the OT and the offset star as determined on the NOT image. However, the STIS image provides more accurate, but slightly different, values for these offsets, so that we can determine exactly how far the object actually is from the slit center. $\Delta\phi_{\rm row}$ represents the difference along the dispersion direction between the two offset determinations. Note that we also checked that the onboard algorithm provided a centroid location for the offset star on the acquisition image consistent, within 0.1 CCD pixels (0.2 MAMA pixels), with the one used to determine the offset between the star and the OT on the STIS CCD image.

Ideally, $\Delta\chi$ is best determined for each scientific data set by cross-correlating its associated wavelength calibration exposure with a prelaunch wavelength calibration exposure.

[19] Throughout this paper, a pixel refers to a native, $1024 \times 1024$ format MAMA pixel, not a "high-resolution" pixel (cf. Woodgate et al. 1998; Kimble et al. 1998).

Unfortunately, the internal lamps were not operated during the prelaunch tests at the same current setting as during the onboard calibration, so the shape of the lamp spectra were too different to be useful. In order to mitigate this effect, we built a template of the prism wavelength calibration lamp at the same setting as used during our observations based on G140L, G230L, and G430L wavelength calibration exposures and the relevant sensitivity curves. However, even this template does not show exactly the same shape at the red end as the wavelength calibration spectrum. The value of $\Delta\chi$ was finally obtained by cross-correlating a 61 pixel long region (along the dispersion direction) of each spectrum where the dispersion is relatively large. As a check, we measured the center of the Ly$\alpha$ geocoronal line determined by the middle position between its edges and found that it falls within one sixth of a pixel of the expected location. Finally, shifts due to thermal or flexure causes were measured to be between 0.02 and 0.2 pixels from orbit to orbit, and thus probably less than 0.1 pixels during an exposure. Finally, regular onboard STIS calibrations enable us to determine $\Delta\beta$ to better than 1/20 CCD pixels (1/10 MAMA pixels). Consequently, a conservative (2 $\sigma$) estimate of the error on the zero point of the wavelength calibration is 0.5 MAMA pixels, or 0.23, 1.4, 5.2, 12, 22, and 29 Å at $\lambda =$ 1200, 1500, 2000, 2500, 3000, and 3300 Å, respectively.

Since the dispersion is small at $\sim$2900 Å (the wavelength of the peak of the sensitivity curve), the effect of the telescope and instrument line spread function (LSF) must be taken into account to obtain a correct estimate of the count rate per pixel. We therefore deconvolved the observed spectrum using the Lucy-Richardson method. Unfortunately, the blending of lines in the wavelength calibration spectrum prevents its use to create an LSF. In the absence of suitable calibration frames taking into account the effect of the point-spread function of the telescope itself, we use an LSF based on the shape perpendicular to the dispersion of the two-dimensional spectrum of the flux standard star HS 2027+0651 at about 2800 Å. Ray-tracing studies indicate that this is a good approximation of the LSF along the dispersion direction (C. W. Bowers 2000, private communication). This star was observed in the prism mode during a STIS calibration program. The immediate consequence is that the corrected (deconvolved) mean level of the count rate is larger by about 25% between 2800 and 3300 Å compared with the uncorrected one.

Before converting the count rate to flux, we checked the wavelength calibration of the prism spectrum of HS 2027+0651 and deconvolved it before building a new sensitivity curve. Once converted to flux, the four individual spectra were rebinned to a same set of wavelengths using bilinear interpolation and averaged. The final, flux-calibrated spectrum of GRB 000301C is presented in Figure 2 (*top*).

### 3.2. *Simulations*

Since Lucy-Richardson deconvolution of a low signal-to-noise ratio (S/N) spectrum actually decreases its S/N, we prefer to compare the spectrum in total observed counts per pixel in wavelength with simulated spectra. These spectra were built using an input spectrum expressed in units of flux, multiplied by the sensitivity curve, integrated over the spectral range of each pixel, and finally convolved with the LSF. The output spectrum expressed in count rate is then multiplied by the exposure time.

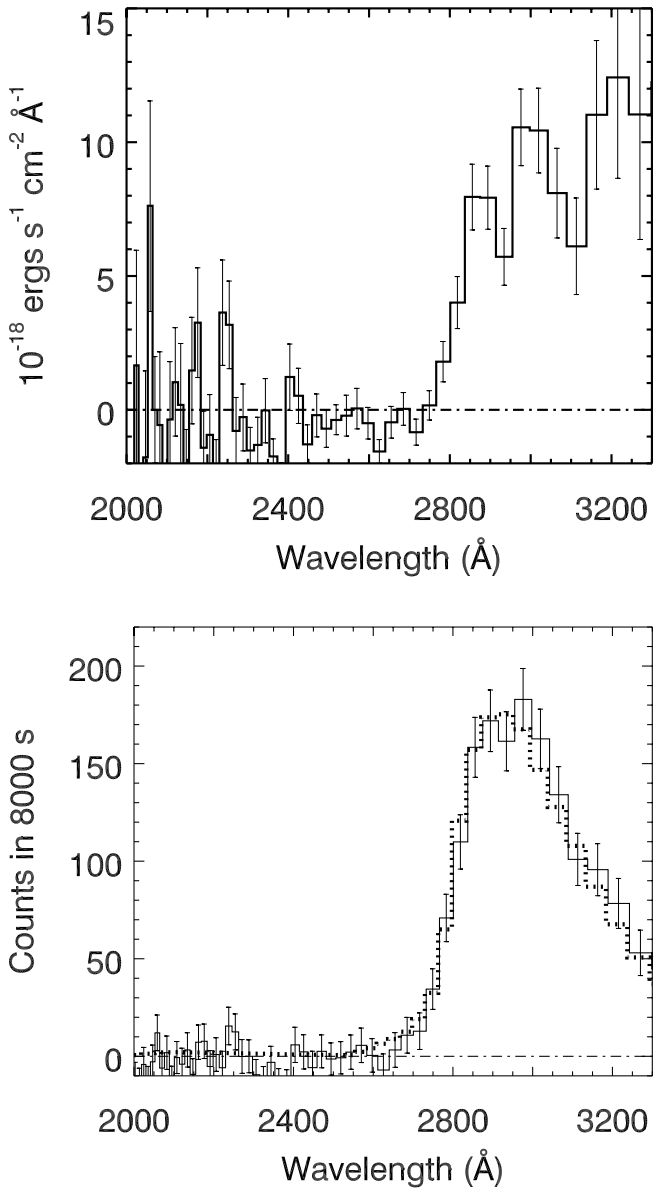


FIG. 2.—*Top*: Deconvolved, flux-calibrated, UV spectrum of GRB 000301C. A break is clearly seen at 2797 Å. If caused by the onset of Lyman continuum absorption due to H I gas associated with the host galaxy, the OT redshift is $z = 2.067 \pm 0.025$. *Bottom*: Comparison of the observed UV spectrum, expressed in observed total number of counts with simulated spectra. The dotted curve corresponds to a model with $\alpha = 0.5$ and extinction by an SMC-like dust with $A_V = 0.15$. A model with $\alpha = 1.2$ and no extinction would present a spectrum indistinguishable in this wavelength range from the one shown here.

In this paper, we only consider input spectra behaving as a power law of the form $f_\nu \propto \nu^{-\alpha}$, as expected for GRB afterglows (Mészáros, Rees, & Papathanassiou 1994; Sari, Piran, & Narayan 1998), modified to take into account the Galactic extinction toward GRB 000301C, the Ly$\alpha$ forest absorption lines, and possible absorption due to H I and $H_2$, as well as extinction by dust located in the host galaxy.

For the Galactic extinction in the direction toward GRB 000301C, we used the value $A_V = 0.16$, as determined from the dust extinction map given by Schlegel et al. (1998) and the analytical expression of the Galactic extinction curve given by Pei (1992).

In order to model the Ly$\alpha$ forest absorption spectrum, we first noted that the likely redshift of GRB 000301C (see below) falls in a range of $1.5 \lesssim z \lesssim 2.3$ where the Ly$\alpha$ forest is still poorly studied. So far, the Hubble Deep Field South (HDF-S) quasar is the only one in that range whose absorption spectrum has been observed at a resolution high enough to determine the H I column density and Doppler parameter by Voigt profile fitting. We thus used the H I absorbers listed by Savaglio et al. (1999) to estimate an absorption spectrum due to their respective Lyman series (Ly$\alpha$ to Ly12) lines. However, we discarded the lines associated with the $z = 1.942$ Lyman limit system seen in the HDF-S quasar, as it is a single event whose occurrence is dominated by small number statistics. Naturally, we also eliminated the lines due to clouds whose redshift is larger than the assumed GRB redshift in the simulation.

Absorption due to H I located in the host galaxy takes into account Lyman series lines, modeled by Voigt profiles, as well as continuous absorption. The redshift of the host galaxy $z$, the H I column density $N_{\rm H\,I}$, and the Doppler parameter $b$ can be easily adjusted. The modeling of possible absorption due to $H_2$ located in the host galaxy follows Draine (2000).

Finally, the possible extinction due to dust in the host galaxy, characterized by the rest-frame $A_V$ extinction and the type of dust (Small Magellanic Cloud, Large Magellanic Cloud, or Milky Way) also uses the expression given by Pei (1992).

### 3.3. *Results*

Figure 2 (*top*) reveals a flat or slightly rising continuum spectrum (in $f_\lambda$) over the range from 2800 Å to the sensitivity-limited red end of the spectrum (3300 Å). No useful constraint on the spectral slope can be derived from the spectrum alone. The mean flux is measured to be $(8.7^{+0.8}_{-1.6} \pm 2.6) \times 10^{-18}$ ergs s$^{-1}$ cm$^{-2}$ Å$^{-1}$, where the first error values come from the uncertainties in the wavelength calibration combined with the strong slope of the sensitivity curve at $\sim$2900 Å; the second error value is the standard deviation of the flux-calibrated error array over the relevant pixels. However, a sharp break can be seen centered at $2797 \pm 25$ Å ($2\,\sigma$). There is no significant flux recovery at the blue end of the spectrum.

### 3.4. *Redshift of GRB 000301C*

The observed break is best interpreted as the onset of continuous absorption below the H I Lyman break due to the presence of a cloud with a large neutral hydrogen column density, located at $z = 2.067 \pm 0.025$ ($2\,\sigma$) in the line of sight to the OT. From the fact that the observed flux is zero within the error bars blueward of the break, we determine that $\log N_{\rm H\,I}({\rm cm}^2) \gtrsim 18.0$. The decreased sensitivity at the blue end combined with the possible presence of other relatively high column density clouds in the Ly$\alpha$ forest does not allow us to set a higher lower limit. An upper limit $\log N_{\rm H\,I}({\rm cm}^2) \leq 23.3$ can be set from the absence of a strong feature at the expected location of the Ly$\beta$ line at $\sim$3100 Å.

Our redshift determination is confirmed by the presence of weakly or marginally detected lines, compatible with Fe II, Mg II, and other low-ionization species at a redshift $z = 2.0335 \pm 0.0003$ in a Keck spectrum obtained by Castro et al. (2000a). More importantly, an ESO Very Large Telescope (VLT) spectrum covering the wavelength range from 3600 to 8220 Å was obtained by Jensen et al. (2001). It reveals a damped Ly$\alpha$ with a large, although uncertain $\log N_{\rm H\,I} = 21.2 \pm 0.5$, within the range allowed by our spectrum, as well as some associated C IV, Fe II, and possibly other low-ionization lines. These lines appear at $z = 2.0404 \pm 0.0008$, a significantly larger value than Castro et al. (2000a) and in reasonable agreement with our value.

The value $z = 2.067 \pm 0.025$ corresponds to the largest direct redshift measurement of the OT to a GRB so far. If we assume that the H I cloud is associated with the OT host galaxy, then the above value is the redshift of the OT. We note, however, that it is conservatively a lower limit to the OT redshift. Indeed, if the object giving rise to the GRB is located outside of a galactic halo or, more generally, in any H I cloud, all the absorption lines detected in the OT spectrum would be due to intervening systems.

Can we set an upper limit to the GRB redshift? Although the ESO VLT spectrum extends down to 3600 Å, its low S/N at the blue end cannot allow us to exclude the presence of low column density Ly$\alpha$ forest lines between 3600 and $\sim$4000 Å. This wavelength corresponds to a firm upper limit of $z = 2.3$ to the GRB redshift. This value also corresponds to the maximal redshift for which our STIS spectrum could reveal Lyman-limit systems, which have $\log N_{\rm H\,I}$ (cm$^2$) $> 17$. Using the number density of Lyman limit systems seen in QSO spectra (Stengler-Larrea et al. 1995) in the relevant redshift range, we estimate that the probability of observing no additional Lyman limit system over the range $2.067 < z < 2.3$ to be 0.68. This value is too small to exclude a redshift larger than $z = 2.067 \pm 0.025$. Similarly, the probability that a random line of sight covering the redshift range $0 < z < 2.3$ would encounter at least one damped Ly$\alpha$ system is $\sim$0.25, based on the number density of damped Ly$\alpha$ systems determined by Rao & Turnshek (2000). This value is too large to ascertain that the redshift of the high column density system corresponds to the redshift of GRB 000301C. In other words, our *HST* STIS spectrum and the ESO VLT spectrum only allow us to limit with certainty the redshift range of the OT to $2.067 < z < 2.3$. However, we can argue in favor of the $z = 2.067 \pm 0.025$ value for the redshift of GRB 000301C. Indeed, on one hand, damped Ly$\alpha$ systems are thought to be mainly caused by merging protogalactic clumps hosted by collapsed dark matter halos and consequently forming stars as the progenitors of normal present-day galaxies (Gardner et al. 1997; Haehnelt, Steinmetz, & Rauch 1998, 2000). On the other hand, most OTs discovered thus far are found to be associated with galaxies (Fruchter et al. 1999b), many of which show signs of significant star formation (Metzger et al. 1997; Djorgovski et al. 1998; Kulkarni et al. 1998; Fruchter et al. 1999a, 1999b; Bloom et al. 1999; Vreeswijk et al. 2001), for which, presumably, a large reservoir of gas is available. In summary, the unusually large H I column density and the fact that most OT host galaxies found so far appear to actively form stars lead us to believe that the absorption seen in the spectrum of GRB 000301C is most likely due to the host galaxy.

### 3.5. *Low Extinction toward GRB 000301C*

When combined with the contemporaneous STIS CCD imaging, the STIS spectrum also allows us to constrain the extinction taking place in the $z = 2.067$ H I cloud toward GRB 000301C. The bottom panel of Figure 2 compares the observed total number of counts with a simulation charac-

terized by an intrinsic power-law spectrum with index $\alpha = 0.5$, as well as some extinction in the host galaxy by SMC-like dust ($A_V = 0.15$). However, in the wavelength range of the STIS spectrum, such a model is indistinguishable from one defined by an intrinsic power-law spectrum with index $\alpha = 1.2$ ($f_\nu \propto \nu^{-\alpha}$) and no extinction in the host galaxy. These two models not only are able to reproduce the appearance of our spectrum without the need of any molecular hydrogen, but also conform to the slope of the optical spectrum (Halpern et al. 2000b; Feng, Wang, & Wheeler 2000; Jensen et al. 2001) within its uncertainty. They also match the count rate of the STIS CCD image within the 15% accuracy of the IDL routine SIM_STIS (P. Plait, 2000 private communication), which predicts the expected count rate for the different STIS modes based on the individual optical components. However, if a steep spectrum with $\alpha = 1.2$ is compatible with our STIS imaging and spectroscopic data alone, a more shallow one ($\alpha \simeq 1$) is favored when ground-based observations with lower uncertainties in optical band magnitudes than the STIS-derived $R$ magnitude are taken into account (cf. Halpern et al. 2000b; Rhoads & Fruchter 2001). Similarly, $\alpha \lesssim 1$ models with low extinction $A_V \lesssim 0.1$ ($A_V \lesssim 0.05$) due to LMC-like (or Milky Way–like) dust are also consistent with the STIS data alone. They predict that the 2175 Å feature (cf., e.g., Blanco, Fonti, & Orofino 1996) should be detectable and shifted to $\sim 6570$ Å. However, its presence seems to be ruled out by existing optical spectra and photometry (Rhoads & Fruchter 2001; Jensen et al. 2001). Therefore, a model with a relatively small amount ($A_V \lesssim 0.1$) of SMC-like dust appears to best fit the full UV-optical data.

## 4. DISCUSSION AND CONCLUSION

The *HST* STIS CCD observations of GRB 000301C revealed a $R = 21.50 \pm 0.15$ source on 2000 March 6.2 (UTC) with no trace of a host galaxy. The NUV-MAMA prism spectrum presents a relatively flat spectrum (in $f_\lambda$) between 2800 and 3300 Å, with a mean flux $(8.7^{+0.8}_{-1.6} \pm 2.6) \times 10^{-18}$ ergs s$^{-1}$ cm$^{-2}$ Å$^{-1}$ and a sharp break centered at $2797 \pm 25$ Å, interpreted as an H I Lyman break. It indicates that the OT arises in or beyond an absorber at $z = 2.067 \pm 0.025$, similar to the ones causing the high column density systems detected in QSO spectra. The redshift and the high H I column density are confirmed by the $\log N_{\rm H\,I} = 21.2 \pm 0.5$ damped Ly$\alpha$, Fe II, C IV, and other lines observed in the ESO VLT spectrum (Jensen et al. 2001a), as well as the Mg II and Fe II lines in the Keck spectrum (Castro et al. 2000a). The lack of a detected host galaxy and the large H I column density system are similar to the situation for damped Ly$\alpha$ systems at $z > 2$ (e.g., Lowenthal et al. 1995; Fynbo, Møller, & Warren 1999), which are thought to be mainly caused by merging protogalactic clumps hosted by collapsed dark matter halos and consequently probe the progenitors of normal present-day galaxies (Gardner et al. 1997; Haehnelt et al. 1998; 2000). Combined with the fact that other OTs are often found in star-forming galaxies, presumably with large H I content, this strongly suggests that $z = 2.067 \pm 0.025$ is actually the redshift of GRB 000301C. If this is the case, our spectrum, as well as the ESO VLT and Keck spectra, suggest that the line of sight to the OT crosses the interstellar medium of its host galaxy.

Our data are compatible with no or little extinction. The absolute magnitude of the OT at the time of the discovery image, 41.5 hr after the burst, was therefore $M_R = -26.1$ for $H_0 = 65$ km s$^{-1}$ Mpc$^{-1}$, $\Omega = 0.3$, and $\Lambda = 0.7$. The low extinction would argue against a naive interpretation that $\gamma$-ray bursts originate in a star-forming region. Instead, one might imagine this favors the hypothesis that GRB 000301C results from a neutron star–neutron star or neutron star–black hole binary merger (Paczyński 1991; Narayan et al. 1992). In this case, this relatively short duration event could have taken place at a significant distance from the host galaxy some time after a significant burst of star formation. Narayan et al. (1992) predict that the median distance between a binary merger and its host galaxy is $\sim 50$ kpc at the time of the burst. Consequently, it is not impossible that the nearby galaxy $\sim 2''$ to the northeast (Rhoads & Fruchter 2000; Kobayashi et al. 2000) is actually the host, although it is very red whereas previous hosts tend to be blue in optical-infrared colors: we derive a $R - K'$ color of $4.9 \pm 0.5$ based on magnitudes measured by Rhoads & Fruchter (2000) and Veillet (2000). In particular, we cannot exclude the possibility that this galaxy lies at $z \sim 2.067$ on the basis of the existing photometry. If this is the case, its H I disk must extend over at least $\sim 20$ kpc ($H_0 = 65$ km s$^{-1}$ Mpc$^{-1}$, $\Omega_0 = 0.3$, and $\Lambda = 0.7$) to cover the line of sight of the OT. This value is similar to the separation between the line of sight to the QSO 2233+131 and the galaxy identified by Djorgovski et al. (1996) as responsible for the $z = 3.150$ damped Ly$\alpha$ in its spectrum. Spectroscopy of the galaxy $\sim 2''$ to the northeast of GRB 000301C is necessary to settle the issue.

However, the present data cannot exclude that the burst itself destroys dust as high-energy photons find their way out of a dense cloud (Waxman & Draine 2000). On the other hand, the time elapsed between the formation of the GRB progenitor and the GRB event itself could be long enough for the progenitor to leave regions of large extinction, as is the case for core-collapse supernovae (Type IIa, Ib/c), a significant fraction of which are also little affected by extinction (e.g., Schmidt et al. 1994). Finally, the low extinction could possibly be explained if the progenitor of GRB 000301C was located in a low-metallicity galaxy that has only recently started to produce stars. The host of GRB 000301C might therefore resemble the galaxies giving rise to damped Ly$\alpha$ absorbers.

*Note added in manuscript.*—After this paper was submitted, the direct determination of the redshift for the optical counterparts of two other GRBs have been reported with redshifts similar to or larger than the one of GRB 000301C: GRB 000926 at $z = 2.037$ (Fynbo et al. 2000b; Castro et al. 2000b) and GRB 000131 at $z = 4.50$ (Andersen et al. 2000).

This work was supported in part by NASA through STIS GTO funding, by STScI GO funding under NASA contract NAS 5-26555, and by the Danish Natural Research Council (SNF). K. H. is grateful for *Ulysses* support under JPL contract 958056, and for *NEAR* support under NAG 5-9503 and NAG 5-3500.

REFERENCES

Andersen, M. I., et al. 2000, A&A, 364, L54
Berger, E., et al. 2000, ApJ, 545, 56
Bernabei, S., et al. 2000, GCN Circ. 599 (http://gcn.gsfc.nasa.gov/gcn3/599.gcn3)
Blanco, A., Fonti, S., & Orofino, V. 1996, ApJ, 462, 1020
Bloom, J. S., Djorgovski, S. G., Kulkarni, S. R., & Frail, D. A. 1998, ApJ, 507, L25
Bloom, J. S., et al. 1999, ApJ, 518, L1
Bloom, J. S., Sigurdsson, S., Wijers, R. A. M. J., Almaini, O., Tanvir, N. R., & Johnson, R. A. 1997, MNRAS, 292, L55
Castro, S. M., et al. 2000a, GCN Circ. 605 (http://gcn.gsfc.nasa.gov/gcn3/605.gcn3)
Castro, S. M., et al. 2000b, GCN Circ. 851 (http://gcn.gsfc.nasa.gov/gcn3/851.gcn3)
Costa, E., et al. 1997, Nature, 387, 783
Djorgovski, S. G., Kulkarni, S. R., Bloom, J. S., Goodrich, R., Frail, D. A., Piro, L., & Palazzi, E. 1998, ApJ, 508, L17
Djorgovski, S. G., Pahre, M. A., Bechtold, J., & Elston, R. 1996, Nature, 382, 234
Draine, B. T. 2000, ApJ, 532, 273
Feng, M., Wang, L., & Wheeler, J. C. 2000, GCN Circ. 607 (http://gcn.gsfc.nasa.gov/gcn3/607.gcn3)
Fruchter, A. S., & Hook, R. N. 1999, PASP, submitted (astro-ph/9808087)
Fruchter, A. S., Hook, R. N., Busko, I. C., & Mutchler, M. 1997, in The 1997 *HST* Calibration Workshop, ed. S. Casertano, R. Jedrzejewski, T. Keyes, & M. Stevens (Baltimore: STScI), 518
Fruchter, A. S., et al. 1999a, ApJ, 516, 683
———. 1999b, ApJ, 519, L13
Fynbo, J. P. U., et al. 2000a, GCN Circ. 570 (http://gcn.gsfc.nasa.gov/gcn3/570.gcn3)
———. 2000b, GCN Circ. 807 (http://gcn.gsfc.nasa.gov/gcn3/807.gcn3)
Fynbo, J. U., Møller, P., & Warren, S. J. 1999, MNRAS, 305, 849
Gardner, J. P., Katz, N., Hernquist, L., & Weinberg, D. H. 1997, ApJ, 484, 31
Garnavich, P., Barmby, P., Jha, S., & Stanek, K. 2000, GCN Circ. 581 (http://gcn.gsfc.nasa.gov/gcn3/581.gcn3)
Garnavich, P. M., Loeb, A., & Stanek, K. Z. 2000, ApJ, 544, L11
Haehnelt, M. G., Steinmetz, M., & Rauch, M. 1998, ApJ, 495, 647
———. 2000, ApJ, 534, 594
Halpern, J. P., et al. 2000a, GCN Circ. 582 (http://gcn.gsfc.nasa.gov/gcn3/582.gcn3)
———. 2000b, GCN Circ. 585 (http://gcn.gsfc.nasa.gov/gcn3/585.gcn3)
Hogg, D. W., & Fruchter, A. S. 1999, ApJ, 520, 54
Jensen, B. L., et al. 2001, A&A, 370, 909
Kimble, R., et al. 1998, ApJ, 492, L83
Klebesadel, R. W., Strong, I. B., & Olson, R. A. 1973, ApJ, 182, L85
Kobayashi, N., et al. 2000, GCN Circ. 587 (http://gcn.gsfc.nasa.gov/gcn3/587.gcn3)
Kulkarni, S. R., et al. 1998, Nature, 393, 35
———. 2000, in Proc. 5th Huntsville Gamma-Ray Burst Symposium, ed. R. M. Kippen, R. S. Mallozzi, & G. J. Fishman (New York: AIP), in press
Leitherer, C., et al. 2000, STIS Instrument Handbook (version 4.1; Baltimore: STScI)
Lindler, D. 1999, CALSTIS Reference Guide (version 6.4; Baltimore: STScI)
Lowenthal, J. D., Hogan, C. J., Green, R. F., Woodgate, B., Caulet, A., Brown, L., & Bechtold, J. 1995, ApJ, 451, 484
Malumuth, E. M., & Bowers, C. W. 1997, in The 1997 *HST* Calibration Workshop, ed. S. Casertano, R. Jedrzejewski, T. Keyes, & M. Stevens (Baltimore: STScI), 144
Meegan, C. A., et al. 1992, Nature, 355, 143
Mészáros, P., Rees, M. J., & Papathanassiou, H. 1994, ApJ, 432, 181
Metzger, M. R., et al. 1997, Nature, 387, 879
Narayan, R., Paczyński, B., & Piran, T. 1992, ApJ, 395, L83
Paczyński, B. 1991, Acta Astron., 41, 257
———. 1998, ApJ, 494, L45
Pei, Y. C. 1992, ApJ, 395, 130
Rao, S. M., & Turnshek, D. A. 2000, ApJS, 130, 1
Rhoads, J., & Fruchter, A. S. 2000, GCN Circ. 586 (http://gcn.gsfc.nasa.gov/gcn3/586.gcn3)
———. 2001, ApJ, 546, 117
Sahu, K. C., et al. 1997, Nature, 387, 476
Sari, R., Piran, T., & Narayan, R. 1998, ApJ, 497, L17
Savaglio, S., et al. 1999, ApJ, 515, L5
Schlegel, D. J., Finkbeiner, D. P., & Davis, M. 1998, ApJ, 500, 525
Schmidt, B. P., et al. 1994, ApJ, 432, 42
Smith, D. A., et al. 1999, ApJ, 526, 683
———. 2000, GCN Circ. 568 (http://gcn.gsfc.nasa.gov/gcn3/568.gcn3)
Stengler-Larrea, E. A., et al. 1995, ApJ, 444, 64
van Paradijs, J., et al. 1997, Nature, 386, 686
Veillet, C. 2000, GCN Circ. 592 (http://gcn.gsfc.nasa.gov/gcn3/592.gcn3)
Vreeswijk, P. M., et al. 2001, ApJ, 546, 672
Waxman, E., & Draine, B. T. 2000, ApJ, 537, 796
Woodgate, B. E., et al. 1998, PASP, 110, 1183